iScience

CellPress
OPEN ACCESS

Article

Silk nanofibrils-MOF composite membranes for pollutant removal from water

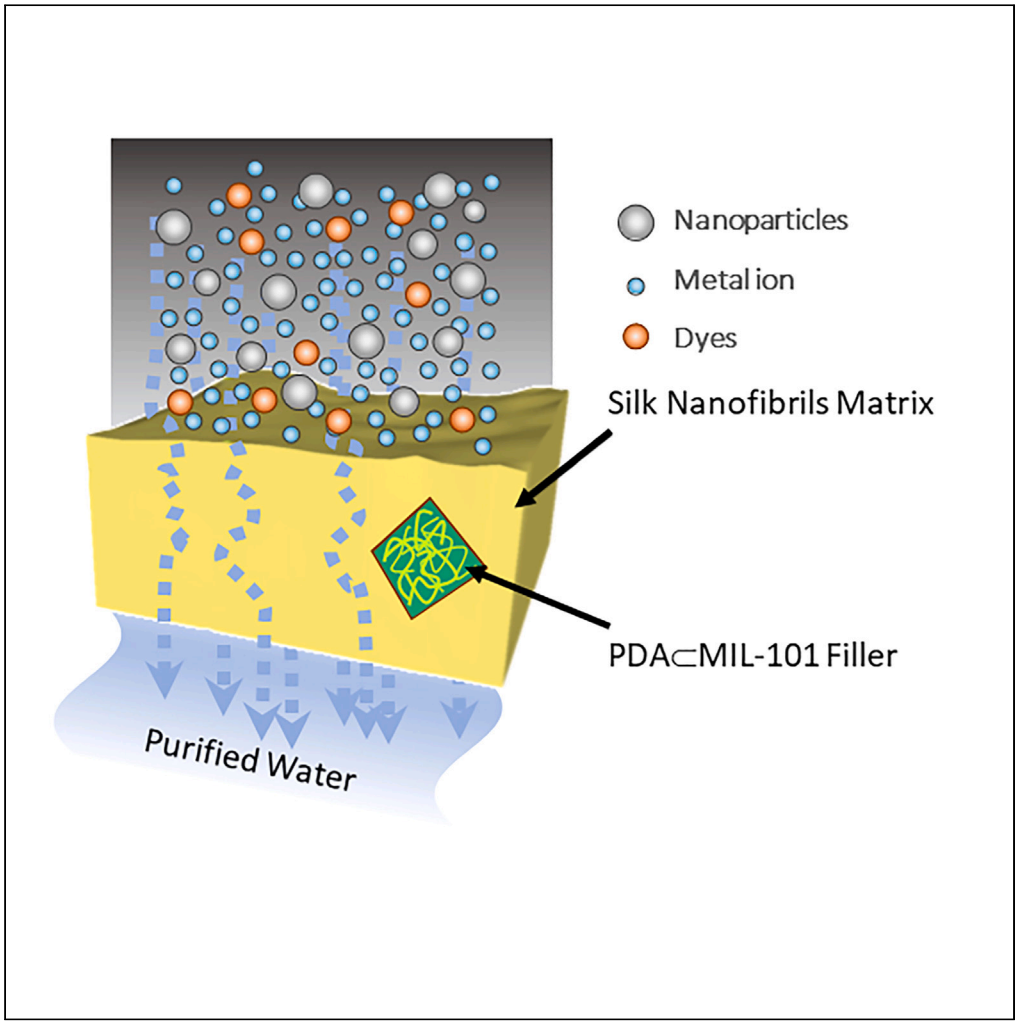

Xiaowen Zhao, Chunhui Wu, Dejun Dai, Jing Ren, Tao Li, Shengjie Ling

litao1@shanghaitech.edu.cn (T.L.)
lingshj@shanghaitech.edu.cn (S.L.)

Highlights

Silk nanofibrils-MOF membranes with high water flux and purification efficiency

The membrane outperforms others in the filtration of heavy metal ions

Nanoparticles and dyes were rejected by over 95%

Zhao et al., iScience 26, 107290
August 18, 2023
https://doi.org/10.1016/j.isci.2023.107290

iScience

CellPress
OPEN ACCESS

Article

Silk nanofibrils-MOF composite membranes for pollutant removal from water

Xiaowen Zhao,[1,3] Chunhui Wu,[1,3] Dejun Dai,[1] Jing Ren,[1] Tao Li,[1,*] and Shengjie Ling[1,2,4,*]

SUMMARY

Membrane separation technology is considered an effective strategy to remove pollutants in sewage. However, it remains a significant challenge to fabricate inexpensive membranes with high purification efficiency. Therefore, the present study proposes the integration of silk nanofibrils (SNFs) and polydopamine⊂metal-organic framework (PDA⊂MOF) nanoparticles to prepare self-supporting membranes, which can effectively intercept nanoparticle pollutants through the size exclusion effect and can strongly adsorb organic dyes and metal ions by SNF. In addition, PDA⊂MOF enables these membranes to adsorb small molecules and heavy metal ions during the filtration process, thereby effectively removing various pollutants from sewage. The integration of size-exclusion and adsorption capabilities enables the SNF/PDA⊂MOF membrane to remove nanoparticles, small-molecule dyes, heavy metal ions, and radioactive elements. This work provides a rational approach for the design and development of the next generation of water treatment membranes and is expected to be used in environmental, food-related, and biomedical fields.

INTRODUCTION

Water pollution by heavy metal ions, dyes, and nuclear waste from industrial production, energy production, and mining has increased dramatically.[1] The World Health Organization (WHO) estimates that in 2017, more than two billion people do not have access to safe drinking water, and 1.2 million people suffer from diseases and impairments due to water pollution.[2–4] A UN report of 2015 predicts that the world will face 40% water scarcity in just 15 years.[5] In particular, highly toxic and small-sized pollutants, including small organic molecules (e.g., dyes, antibiotics, and pesticides), heavy metals (e.g., cadmium, chromium, lead, arsenic, and mercury), and radioactive elements (e.g., uranium) have been proven to be the pollutants that have the most significant impact on human health and cause the most serious damage to the ecological environment.[1] In this article, these pollutants are referred to as small-sized and highly toxic contaminants and abbreviated as soluble harmful pollutants (SHPs). These SHPs can cause severe organ damage, congenital disabilities, and cancer, even at relatively low concentrations. Only a limited number of methods are capable to remove SHPs, including physical/chemical adsorption, reverse osmosis technology, and electrocatalytic- and photocatalytic-based treatments.[6] However, these methods and technologies still have deficiencies. For example, the applied adsorbents typically have poor cycle stability and low efficiencies, and the types of pollutants that can be adsorbed by one specific adsorbent are limited. Reverse osmosis technology, instead, is expensive and cumbersome to operate, and the amount of water it can treat is quite limited. Furthermore, electrocatalytic- and photocatalytic-based methods are difficult to upscale for industrial applications.

These issues have motivated the development of membranes for water treatment as they are energy-efficient techniques for removing SHPs.[6–8] To date, a range of new materials (e.g., polymers,[9–11] biomaterials,[12–15] inorganic nanomaterials,[16–24] metal-organic frameworks,[25–31] and covalent organic frameworks[32–34]) and advanced fabrication methods (e.g., block copolymer self-assembly,[9] dual-interface engineering methods,[35,36] orbital etching techniques,[16,37] chemical vapor-phase deposition,[38,39] and layer-by-layer assembly[40,41]) have been developed for the preparation of water treatment membranes (WTMs). However, preparing low-cost WTMs with high water flux and high purification performance remains a significant challenge. For example, various layered inorganic nanosheets, such as graphene oxide,[23] molybdenum disulfide,[19] and tungsten disulfide,[18] have been used to construct layered WTMs. However, to achieve an effective removal of SHPs, it is necessary to create nanochannels in these nanomaterials

[1]School of Physical Science and Technology, ShanghaiTech University, Shanghai 201210, China

[2]Shanghai Clinical Research and Trial Center, Shanghai 201210, China

[3]These authors contributed equally

[4]Lead contact

*Correspondence: litao1@shanghaitech.edu.cn (T.L.), lingshj@shanghaitech.edu.cn (S.L.)

https://doi.org/10.1016/j.isci.2023.107290

through post-synthetic modification (surface modification, ion exchange, addition of foreign species), grafting, or impregnation.[42] These techniques are complex and costly, thereby impeding the commercialization of these membranes.

Adsorption membranes designed to exploit the adsorption properties of inorganic nanomaterials for SHPs have become a possible alternative, especially porous adsorption membranes based on metal-organic frameworks (MOFs), which have received extensive attention in recent years. A large number of water stabilized MOF, UiO-66,[43] NU-1000,[44] MOF-808,[45] and MIL-100[30] have been reported successively for the preparation of WTMs. The pore size, pore geometry, and pore chemistry of MOFs can be precisely tuned at the sub-Angstrom level. In addition, the strong adsorption sites present in high density within MOFs are susceptible to post-synthetic modification to improve adsorption specificity and diversity.[27] In addition, guest materials with high adsorption capacity for SHPs can also be introduced into the MOF channels to enhance adsorption efficiency. For example, Queen et al. introduced polydopamine (PDA) with high metal adsorption capacity into MIL-100(Fe) to enhance its adsorption capacity for heavy metals, such as bivalent lead and mercury cations.[29] The metal ions captured by PDA are confined in MIL-100(Fe), so they can be well separated and extracted during subsequent processing, allowing the reuse of precious metals. However, the membrane formed by MOFs is mechanically weak and usually needs to be filled in or supported by other matrix materials.[46] As a result, the advantages of MOFs of ultrahigh specific surface area and selective adsorption are significantly compromised.

In addition to laminated inorganic nanomaterials, biopolymers (such as cellulose, chitin, and proteins) are also widely used to fabricate filtration membranes due to their advantages regarding costs, environmental friendliness, and biocompatibility. However, these membranes mainly rely on the size of the nanochannels formed between the nanofibers to reject pollutants. Therefore, they usually only retain nanoparticles or contaminants larger than a few nanometers and are ineffective for the removal of SHPs.[13,47] This problem is expected to be solved by integrating biopolymers and MOFs in one membrane system. First, such composite membranes can effectively intercept nanosized pollutants through size exclusion, that is, they have the function of ultrafiltration membranes.[35] Second, the effective removal of various SHPs from sewage can be achieved through the adsorption of these pollutants by biopolymers and MOFs.

According to this strategy, this study presents an approach to develop a self-supporting composite membrane for sewage treatment. The membrane is formed by integrating silk nanofibrils (SNFs) and PDA-decorated MIL-101(Cr) (PDA⊂MIL-101(Cr)) nanoparticles, two nanomaterials with strong adsorption capabilities for various pollutants. The PDA is encapsulated in MIL-101(Cr) pores using a previously reported double solvent method, and the SNFs form a self-supporting structural framework during filtration (Figures 1A and S2).[48] The developed membrane has a pore size range of 3–10 nm, which enables it to intercept nanoparticle pollutants through the size exclusion effect. Additionally, the SNF protein component provides chemical sites for dye adsorption. The membrane can remove a wide range of pollutants present in sewage, including small-molecule dyes, heavy metal ions, and radioactive elements, resulting in a highly efficient membrane. The embedded mesoporous PDA⊂MIL-101(Cr) nanoparticles provide additional free volume to expedite fluid diffusion and enhance the membrane's ability to adsorb heavy metal ions and radioactive elements, greatly improving its compatibility and broad application potential. This work introduces a new idea for designing and developing a new generation of WTM technology with enhanced efficiency, high-water flux, and broad application potential. The developed membrane is expected to be used in environmental, food-related, and biomedical fields.

RESULTS AND DISCUSSION

Preparation of MIL-101(Cr) and PDA⊂MIL-101(Cr)

MOFs, such as UiO-66,[25–27] ZIF-8,[28] MIL-100(Fe),[29,30] and MIL-101(Cr),[31] have been used for the adsorption of heavy metal ions in sewage. Recently, the MIL-101 series were frequently employed either in composites or as pristine materials for the removal of toxic metals or organic pollutants because of their excellent hydrothermal stability, rigid architecture, high porosity, high specific surface area, and facile chemical modification.[31,42,49] MIL-101(Cr) has a very large Brunauer–Emmett–Teller (BET) surface area (3163 $m^2\ g^{-1}$ measured by nitrogen adsorption, Figure 1E and Table S2) and numerous unsaturated chromium sites (up to 3.0 mmol g^{-1}) for potential adsorption of pollutants.[49–51] These sites can be chelated by compounds with electron-rich organic groups, thereby enhancing the selective adsorption capacity for SHPs. Functionalization, metal doping into the MIL-101 structure, and incorporating other materials are three strategies to

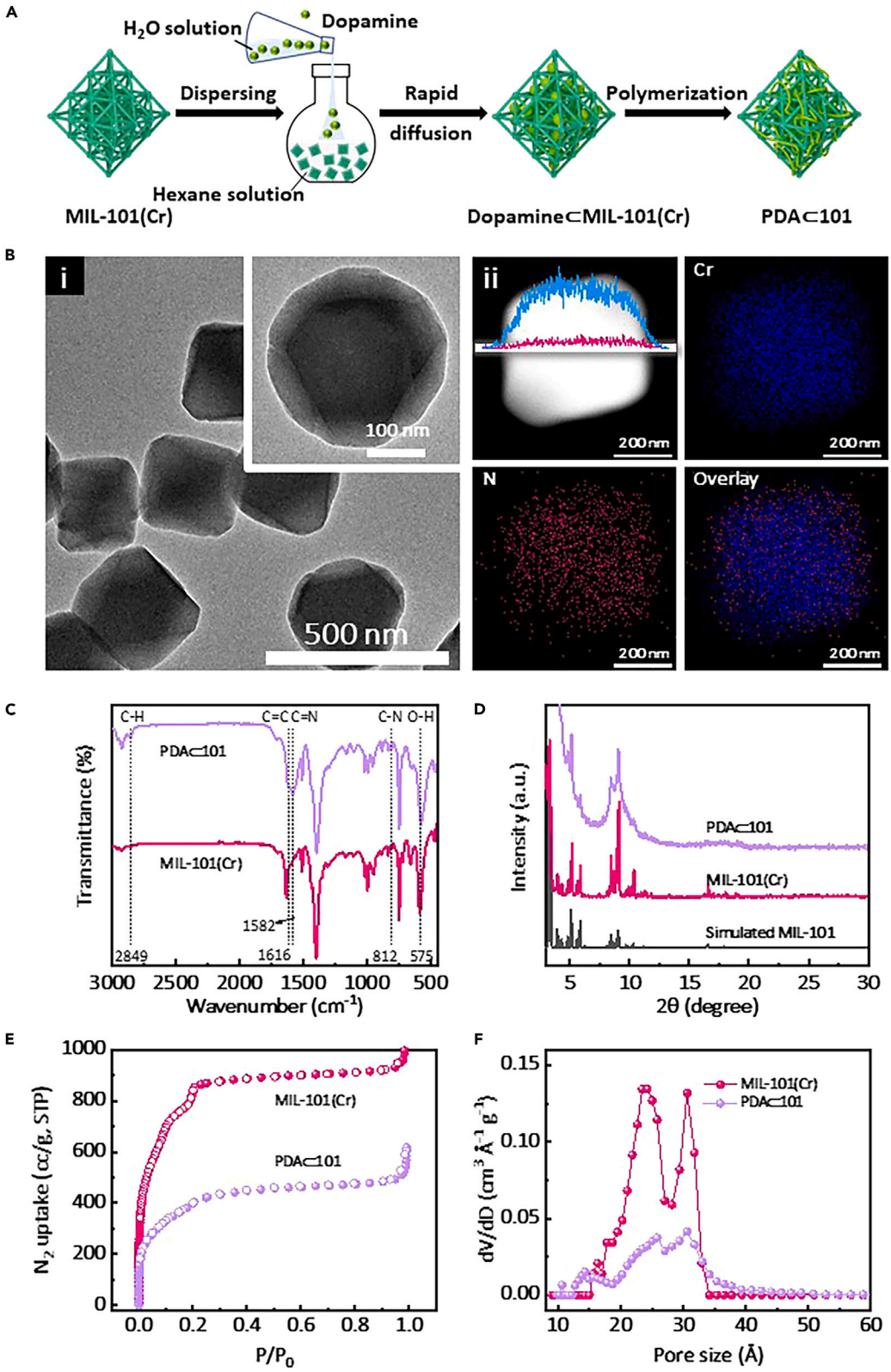
A
H2O solution
Dopamine
Dispersing
Rapid
diffusion
Polymerization
Hexane solution
MIL-101(Cr)
Dopamine⊂MIL-101(Cr)
PDA⊂101
B
i
100 nm
500 nm
ii
200 nm
Cr
200 nm
N
200 nm
Overlay
200 nm
C
C-H
C=C C=N
C-N O-H
PDA⊂101
MIL-101(Cr)
1582
2849
1616
812
575
Transmittance (%)
3000 2500 2000 1500 1000 500
Wavenumber (cm-1)
D
PDA⊂101
MIL-101(Cr)
Simulated MIL-101
Intensity (a.u.)
5 10 15 20 25 30
2θ (degree)
E
MIL-101(Cr)
PDA⊂101
N2 uptake (cc/g, STP)
0 200 400 600 800 1000
0.0 0.2 0.4 0.6 0.8 1.0
P/P0
F
MIL-101(Cr)
PDA⊂101
dV/dD (cm3 Å-1 g-1)
0.00 0.05 0.10 0.15
10 20 30 40 50 60
Pore size (Å)

Figure 1. Preparation and properties of MIL-101(Cr) and PDA⊂MIL-101(Cr) (specifically: PDA⊂101(18))
(A) Scheme of the synthesis of PDA⊂MIL-101(Cr).
(B) TEM images (i) and EDS elemental mapping (ii) of PDA⊂MIL-101(Cr).
(C) FT-IR spectra of MIL-101(Cr) and PDA⊂MIL-101(Cr).
(D) PXRD patterns of MIL-101(Cr) and PDA⊂MIL-101(Cr).
(E) Nitrogen adsorption–desorption isotherms at 77 K of MIL-101(Cr) and PDA⊂MIL-101(Cr).
(F) Pore size distribution profiles of MIL-101(Cr) and PDA⊂MIL-101(Cr).

enhance the adsorption capacity of MIL-101. In addition, the toxicity of Cr depends on its oxidation state, and Cr(III) in the MIL-101(Cr) is relatively nontoxic.[52] Therefore, MIL-101(Cr)-based materials were one of the most frequently reported MOF-based adsorption materials in recent literature. For example, the methyl orange adsorption capacity of a graphite oxide/MIL-101(Cr) hybrid was 235 mg g^{-1}, and MIL-101(Cr)-NH_2 demonstrated a chromium(VI) adsorption capacity of 44 mg g^{-1}.[53,54] MIL-101(Cr) was also functionalized by the amidoxime group to improve the selective adsorption of hexavalent uranium.[55] However, these strategies can only achieve the selective adsorption of a few types of pollutants and cannot meet the removal requirements of a broad spectrum of SHPs.

To enhance the broad-spectrum adsorption capacity of MIL-101 for SHPs, this study uses a previously reported post-synthetic modification strategy to increase the number of accessible adsorption sites of MIL-101 for SHPs. MIL-101 is characterized by larger pore sizes with diameters of 29 and 34 Å, and pore apertures of 12 and 16 Å, respectively, making it suitable for the irrigation of polymer monomers and improving the success rate and load of polymer combination in the composite material.[49–51] In this study, PDA was introduced into the pores of MIL-101(Cr) (Figure 1A) via post-synthetic modification. The involvement of PDA thus provides the MIL-101 with more adsorption sites as PDA is rich in amino/imino and hydroxyl functional groups.[56] Monodispersed MIL-101(Cr) particles with an average size of 400 nm and 200 nm were synthesized according to a previously reported method with slight modifications (Figure S1).[57] N_2 adsorption experiments were conducted, and the results showed a limited impact of particle size on BET surface area (Figure S1). If not specified, MIL-101(Cr) with a size of 400 nm was used for the subsequent tests. Because MIL-101(Cr) lacks open metal coordination sites, the *in-situ* polymerization techniques reported by Queen et al.[30] cannot be applied here. The double solvent method, another methodology also demonstrated by Queen et al., was reported to increase the amount of dopamine precursor that diffused into the pores, inhibiting polymerization on the outer surface of MIL-101(Cr).[48] According to this method, dry MIL-101(Cr) particles were soaked in anhydrous hexane, which was followed by the addition of a small amount of an aqueous solution containing dopamine hydrochloride. Then, a diluted aqueous ammonia solution was added to the mixture to induce dopamine polymerization. After 9 h, the resulting composite PDA⊂MIL-101(Cr) was washed and dried (Figure 1B).

Characterization of PDA⊂MIL-101(Cr) and PDA⊂MIL-101(Cr)

The Fourier transform infrared (FT-IR) spectra of PDA⊂MIL-101(Cr) confirmed the successful polymerization of dopamine to PDA (Figure 1C). The peak in the spectrum of PDA⊂MIL-101(Cr) at 1582 cm^{-1} corresponds to the vibration of the C=N and C=C groups in PDA.[58] Transmission electron microscopy (TEM) images showed that the particle surfaces of the obtained PDA⊂MIL-101(Cr) material were very clean and smooth, suggesting that PDA resides within the cavities of MIL-101(Cr) rather than on its surface (Figures 1B(i) and S2B). Energy-dispersive X-ray spectroscopy (EDS) elemental mapping result and line scan result showed that nitrogen present in PDA was evenly distributed in the cavity of the MOF particle (Figure 1B(ii)). The N 1s region of the X-ray photoelectron spectroscopy (XPS) spectra of PDA⊂MIL-101(Cr) presence of the secondary and tertiary amines, which did not find in the spectrum of MIL-101(Cr), also indicating that polymer is indeed present inside the MOF cavities (Figure S2C). Powder X-ray diffraction (PXRD) analysis revealed that the characteristic peaks of PDA⊂MIL-101(Cr) matched well with the theoretically fitted characteristic peaks of MIL-101(Cr), indicating that the crystallinity of the MOF was fully maintained after the involvement of PDA (Figure 1D). MIL-101(Cr) and PDA⊂MIL-101 demonstrate excellent hydrolytic stability when stored in water, with almost no detection of Cr even after six months (Figure S3 and Table S2). The PDA loading was determined to be 17.8 wt % (denoted as PDA⊂101(18) from here) by thermogravimetric analysis (TGA) (Figure S2D and Table S1).

Then, we investigated the sorption properties of PDA⊂MIL-101(Cr). The nitrogen sorption isotherms of MIL-101(Cr) and PDA⊂101(18) were measured at 77 K to evaluate the pore volume change after the encapsulation of PDA. PDA⊂101(18) exhibited a nitrogen uptake capacity of 602 cm^3 g^{-1} at 0.99 bar with the

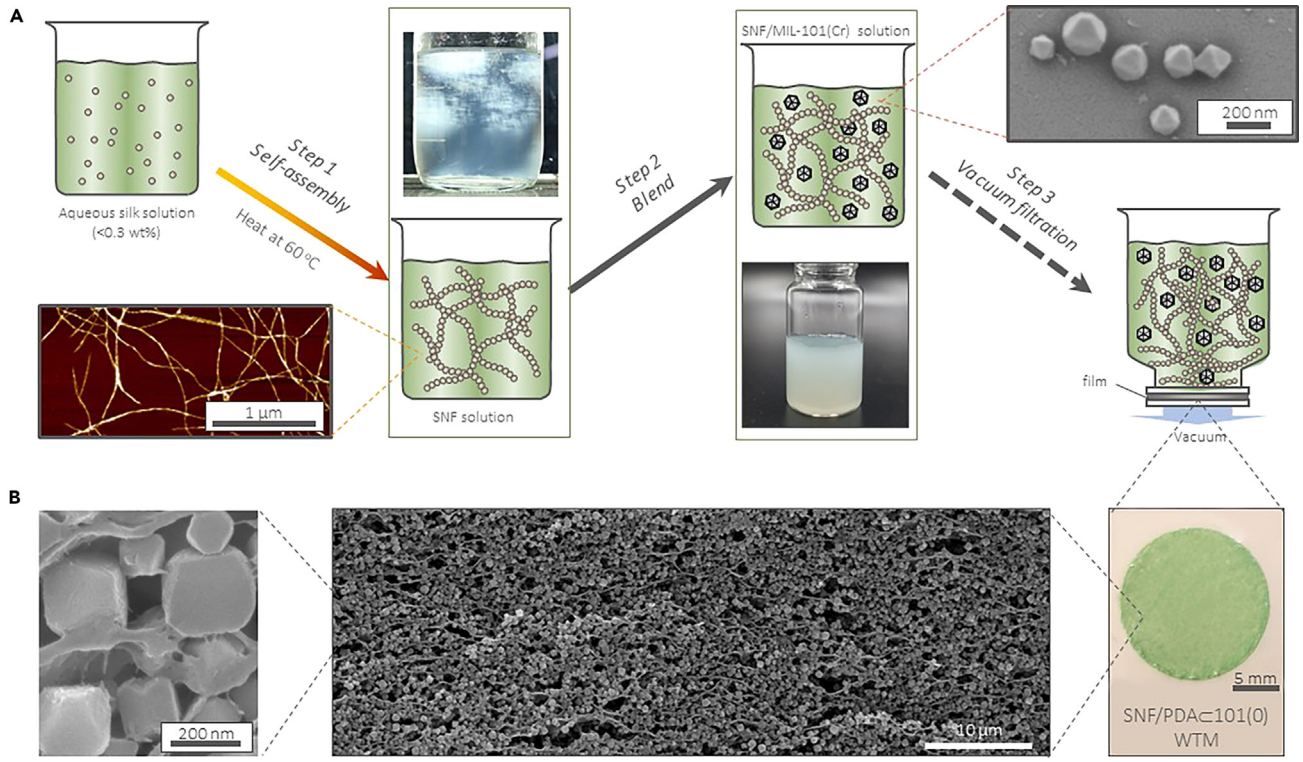

Figure 2. General pathway to fabricate SNF/PDA⊂101 WTMs (specifically: SNF/PDA⊂101(0) WTM)

(A) Schematic of the preparation steps for SNF/PDA⊂101 WTMs. Step 1: Assembly of silk to SNFs in aqueous solution. The first column, the bottom: atomic force microscopy (AFM) image of the SNFs; the second column, the top: photograph of the SNF solution under polarized light, indicating the presence of a nematic phase of SNFs. Step 2: Mixture of MOF and SNF solution. The third column, bottom: is a photograph of the SNF/MIL-101(Cr) solution; the fourth column, top: SEM image of MIL-101(Cr). Step 3: Assembly of SNF/MIL-101(Cr) dispersions into membranes via vacuum filtration.

(B) Structures of the membranes. Right: photograph of an SNF/PDA⊂101 WTM with a thickness of 67 μm; middle: cross-sectional SEM image of an SNF/PDA⊂101 WTM; left: high-resolution cross-sectional SEM image of the SNF/PDA⊂101 WTM.

isotherm normalized to MIL-101(Cr), which was lower than that of pristine MIL-101(Cr) (1160 $cm^3\ g^{-1}$) (Figure 1E). The pore size distribution showed that MIL-101(Cr) had two types of mesopores with free diameters of ca. 24 Å and 30 Å. However, a new narrow pore of 1.5 nm in diameter was observed for PDA⊂MIL-101(Cr), and the calculated pore volume of PDA⊂101(18) (0.931 cc g^{-1}) was decreased compared to that of MIL-101(Cr) (1.795 cc g^{-1}) (Figure 1F and Table S2). Thus, it is reasonable to conclude that the reduction in nitrogen uptake capacity is a result of reduced pore volume due to the introduction of polymer in the pore.

Assembly of SNF/PDA⊂101 WTMs

SNF/PDA⊂101 WTMs were prepared by vacuum filtration of an aqueous dispersion of SNFs prepared by thermally induced self-assembly and MIL-101(Cr) or PDA⊂MIL-101(Cr) (Figure 2A).[59] Since SNFs are stable in an aqueous solution as a nematic network structure, the fibrils can confine water-dispersed MIL-101(Cr) or PDA⊂MIL-101(Cr) in their nano-network, achieving uniform dispersion of the hybrid. Therefore, the SNF/MOF dispersion can be stable at room temperature for more than 15 days without flocculation, delamination, and aggregation (Figure S3C). This dispersion can be assembled into a self-supporting and water-insoluble membrane through vacuum filtration (Figure 2A). Neither membrane dissociation nor breakage was observed, even when the membrane was soaked in pure water for up to 100 days (Figure S3D). For SNF dispersions, it usually takes up to 12 h to form a self-supporting membrane because when the initially settled SNFs form a thin film layer, only a limited number of channels are present to allow water to pass through, which will significantly constrain the water flux. With the increase in membrane thickness, the reduction in water flux will become more significant. Unlike the pristine SNF system, MOF particles provided a large number of additional nanochannels for water transport. Thus, the membrane formation

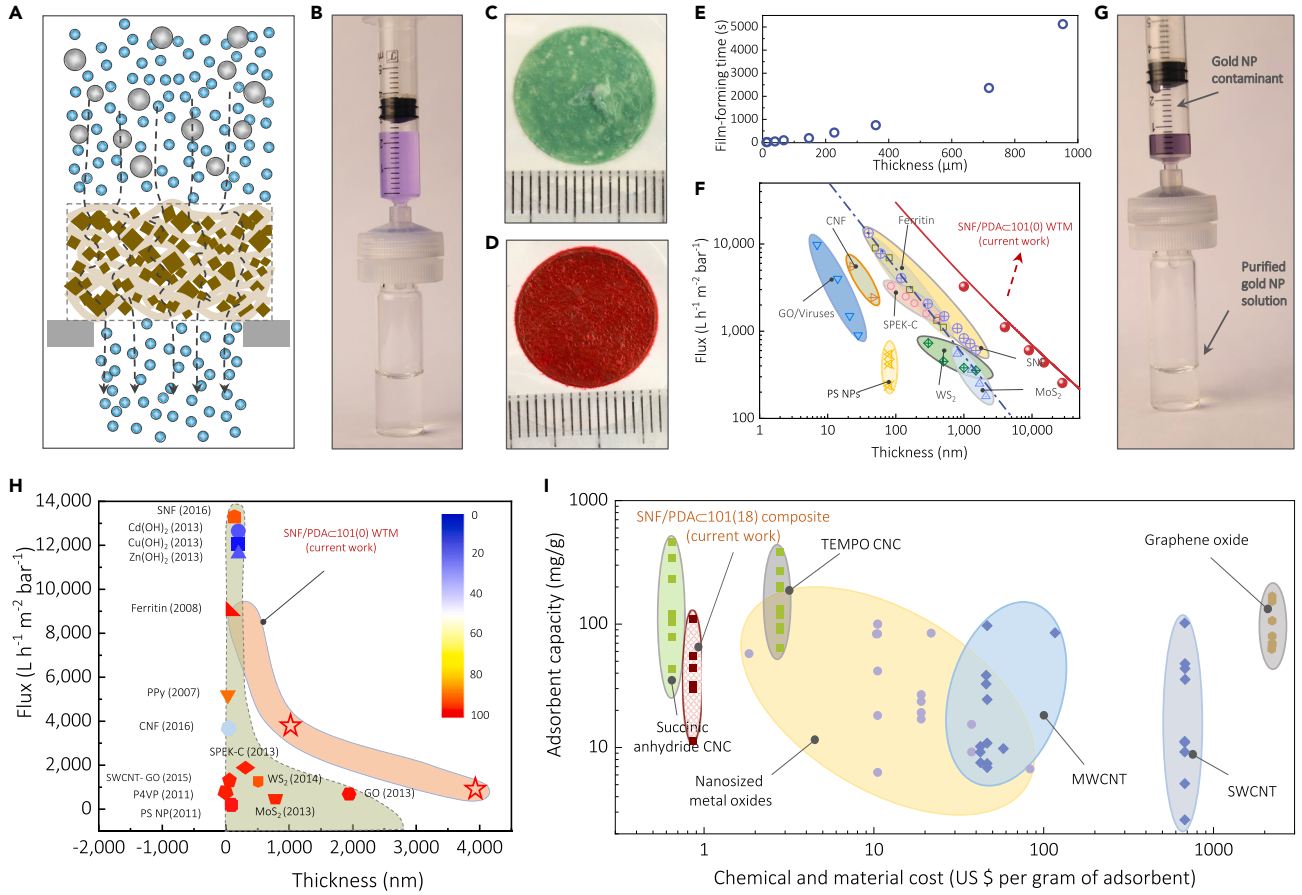

Figure 3. Separation performance of SNF/101 WTMs

(A) Cross-sectional representation of filtering an aqueous (blue circles) pollutant (gray circles) mixture through SNF/101 WTM.

(B) Image of the SNF/101(0) syringe nanofiltration, which successfully removed Coomassie Brilliant Blue R with a rejection of 100%.

(C) SNF/101(0) WTMs before filtration of 10 mL of a 128-μM Eosin B solution.

(D) SNF/101(0) WTMs after filtration of 10 mL of a 128-μM Eosin B solution.

(E) Relationship between film thickness and film-formation processing time.

(F) Thickness-dependent changes in permeability to pure water for the SNF/101(0) WTMs and other previously reported membranes. The line is a fitted curve using the Hagen-Poiseuille equation with a uniform structure.[14,60]

(G) Photographic image of the SNF/101(0) syringe nanofiltration, which successfully removed gold nanoparticles with a rejection of 100%.

(H) Comparison of the 13-nm gold nanoparticle separation performance of SNF/101(0) WTM to that of other filtration membrane materials. The rejection is represented by the color of the pattern. Blue and red indicate 0 and 100% rejection, respectively.

(I) Cost and adsorption capacity estimate for the most-studied nanomaterials.

from an SNF/MOF dispersion is relatively fast. For example, a 12-μm thick film can be fabricated in only 13.3 s when using a reduced pressure of 80 kPa (Figure 3E).

The cross-sectional scanning electron microscopy (SEM) images of SNF/MIL-101(Cr) (denoted as SNF/PDA⊂101(0) WTM from here) revealed that the MOF nanoparticles were uniformly dispersed in the SNF matrix (Figures 2B and S4A). The uniform three-dimensional skeleton structure composed of SNF provides a stable framework for the MOF particles, preventing their leaching. This is likely due to the excellent mechanical strength and flexibility of SNFs,[61] which allow them to form physical entanglements with the MOF particles and hold them tightly in place. Therefore, subsequent vacuum operations will not significantly affect the morphology and density of the membrane (Figure S4B and Table S3). On the other hand, the thickness of the membranes can be adjusted by the amount of dispersion used for vacuum filtration (Figure 3E). As illustrated in Figures S4C–S4E, the dispersion dosage and the thickness of the resulting membrane exhibited a good positive linear correlation in the dosage range of 0–30 mL. The excellent mechanical flexibility of SNF/PDA⊂101 WTMs is demonstrated in Figures S4F and S4G, where a membrane with a

diameter of 15 mm can be bent without breakage and can be cut into desired shapes. Although a higher mass ratio of MOF improves filtration efficiency, it can also decrease the membrane's mechanical properties, as shown in Figure S4H. To strike a balance between the two factors, we carefully selected the membrane with the highest content of MOF that still maintained good mechanical stability. This ensures that the membrane can be easily handled without breaking down during experiments, while still achieving optimal filtration performance. Such strong and tough mechanical properties benefit WTMs, allowing membranes to be operated in the filtration process under high hydrostatic pressure conditions. In contrast, some brittle WTMs, such as membranes consisting of inorganic nanofibers or nanowires, as well as nanosheet-based membranes, usually need to be further integrated into support materials to withstand pressure-driven filtration operations. In addition to vacuum filtration, SNF/MOF dispersions can also form WTMs on the surface of a microfiltration membrane by syringe extrusion (Figure 3B and Video S1). The high-water permeability of the SNF/MOF hybrid allows the membrane to be formed without the use of any pressure-driven device, and self-supporting high-permeability WTMs can be assembled on syringe filters by manual extrusion. SNFs in dispersion exist as three-dimensional interconnected nematic networks, thus even though the sizes of MIL-101(Cr), PDA⊂101(18), and SNF are 55 times smaller than the pore size of the microfiltration membrane, the component mixture did not pass through the microfiltration membrane during the extrusion process but deposited on the surface of the microfiltration membrane to form a composite membrane. Such freshly prepared membranes can be directly used to isolate small-molecule dyes. This facile and rapid membrane formation method is beneficial to the practical application of WTMs as it can substantially reduce manufacturing costs and adapt to more diverse usage requirements. However, in evaluating the water flux and retention effect of SNF/PDA⊂101 WTMs dominated by the size exclusion effect, we mainly focus on the SNF/PDA⊂101(0) WTM because MOF is a dispersion phase. The pore size of SNF/PDA⊂101 WTMs is dominated by the SNF network and the ratio between SNF and MOF particles.

Evaluation of the water flux of SNF/PDA⊂101 WTMs

As shown in Figure 3F, the pure water flux of 1-μm thick SNF/PDA⊂101(0) WTM is as high as 3249 L h^{-1} m^{-2} bar^{-1}, which is more than 400 times higher than that of commercial filtration membranes and more than four times higher than that of recently reported state-of-the-art ultrafiltration membranes of similar thicknesses, such as polystyrene nanoparticle membranes, covalent organic framework membranes, tungsten disulfide membranes, and graphene oxide membranes[14,18,19,21,22,33,62–66] (Table S4). The highest water flux of the ultrathin SNF membrane can reach 8355 L h^{-1} m^{-2} bar^{-1}. However, the thickness of these membranes was below 50 nm. These ultrathin membranes can only intercept pollutants through the size exclusion effect, so increasing the thickness of the membrane will inevitably lead to a sharp drop in water flux, manifested as a greater downslope than observed for other WTMs. In contrast, due to the uniform dispersion of MOF particles in the membrane, a large number of free-volume channels are provided for water transport, thus significantly reducing the dependence of water flux on membrane thickness. As shown in Figure 3H, the water flux decreased with thickness more moderately than other WTMs. Therefore, even when the thickness of the SNF/PDA⊂101(0) WTM increased to 23 μm, its water flux remained at 70 L h^{-1} m^{-2} bar^{-1}. This water flux is still comparable to other ultrathin membranes, like molybdenum disulfide membranes, tungsten disulfide membranes, and polystyrene nanoparticle membranes.[62] In addition, the dependency of water flux on the thickness of SNF/PDA⊂101(0) WTM can be well described by the mechanical model of the composite structure (Figure 3F and Equation 1). Compared with the single-component model, the hybrid structure model has been shown to substantially increase the water flux for the same size and film thickness. The design concept of SNF/PDA⊂101(0) WTMs is the simultaneous utilization of the size exclusion of membranes and the adsorption of SHPs by membrane components to purify the sewage. Therefore, it is beneficial to moderately increase the thickness of the membrane, which can substantially improve its adsorption capacity.

Rejection of nanoparticles and dyes by SNF/PDA⊂101 WTMs

Nanoparticles of different sizes were first selected to verify the retention efficiency of the SNF/PDA⊂101 WTMs. As summarized in Table 1, whether it is gold nanoparticles with diameters of 15.5 ± 4.0 nm (Figures 3G and S5C and Video S2) or platinum nanoparticles with diameters of 3 nm (Figure S5A), the rejection by the SNF/PDA⊂101(0) WTM is 100%, indicating that SNF/PDA⊂101 WTMs can effectively remove substances with sizes greater than 3 nm through size exclusion. Common nanoparticle pollutants in water, such as bacteria, viruses, and inorganic nanoparticles, are much larger than this scale, so they can all be rejected by SNF/PDA⊂101 WTMs. However, in addition to nanoparticle pollutants, sewage usually contains SHPs. The content of these substances in sewage is generally low, usually below ppm level, but their

Table 1. Separation performance of 240-μm-thick SNF/101(0) WTM for dyes and nanoparticles

	Mw (g mol $^{-1}$)	Size (nm)	Concentration	Charge	Flux (L h^{-1} m^{-2} bar^{-1})	Rejection (%)
Pt nanoparticles	195.05	3 nm	24.3 mg mL^{-1}	–	38.8	100
Pt nanoparticles	195.03	10 nm	24.3 mg mL^{-1}	–	38.9	99.7
Au nanoparticles	196.97	13 nm	200 mg mL^{-1}	–	38.7	100
Eosin B	624.06	1.1 × 1.0	128 μM	–	55.5	94.5
Orange G	452.4	1.3 × 0.8	240 μM	–	45.8	99.5
Alcian blue 8GX	1298.88	2.5 × 2.3	22.6 μM	+	35.4	100
Brilliant Blue R	825.97	1.7 × 1.8	199 μM	–	35.6	99.1
Brilliant Blue G	854.04	2.3 × 1.8	139 μM	–	36.8	95.7
Rhodamine B	479.01	1.6 × 1.3	5 μM	+	39.8	99.5
Congo Red	696.66	1.9 × 1.3	17 μM	–	55.8	100
Direct Red 81	1373.07	2.4 × 0.8	120 μM	–	39.3	96.4

The flux listed in the table was calculated from the filtration of model compound solutions. The filtration pressure was kept at 80 kPa in all these tests. Several dye solutions have lower flux than pure water, likely because of their large molecular size, which would be responsible for blocking the membrane pores.

environmental toxicity and harm to human health are the most serious. For example, mercury content in water exceeding 3.0 × 10^{-5} ppm can cause impairment to the lung and kidneys, chest pain, and dyspnea.[67] Similarly, if the lead content in water exceeds 6.0 × 10^{-3} ppm, it may cause damage to the central nervous system.[68]

Due to the strong adsorption capacity of SNF and MIL-101 series nanoparticles for SHPs, SNF/PDA⊂101 WTMs should be capable of removing SHPs from sewage. To this end, various organic small-molecule dyes, such as Eosin B, Orange G, and Alcian blue 8GX, were selected to verify this inference. These dyes differ in size between 0.8 and 2.5 nm, which is significantly smaller than the pore size of SNF/PDA⊂101 WTMs. However, the results summarized in Table 1 reveal that SNF/PDA⊂101 WTMs effectively intercept these small molecules. Furthermore, the rejection is independent of whether they are positively or negatively charged. For example, SNF/PDA⊂101(0) WTM achieved 99.5% retention for 240-μM Orange G and 99.1% retention for 199-μM Coomassie Brilliant Blue R. However, in a comparable dye concentration range, previously reported ultrafiltration membranes with similar pore sizes, such as graphene oxide membranes, covalent organic framework membranes, and molecularly porous cross-linked membranes,[69] generally have a rejection rate of less than 80% for these dyes.

Our results indicated that the amount (204 mg g^{-1}) of dyes (Coomassie Brilliant Blue R as an example) that SNF/PDA⊂101(0) WTM could reject was much higher than the adsorption capacities of SNFs and MIL-101(Cr). Therefore, we speculate that the initial interaction of SNF/PDA⊂101 WTMs with dyes mainly depends on their adsorption by SNF and MIL-101 series particles. In this process, these adsorbed dyes gradually fill the membrane channels and progressively accumulate on the membrane surface to form a filter cake, thereby reducing the pore size of SNF/PDA⊂101 WTMs. The SNF/PDA⊂101 WTMs with reduced pore size can thus reject dyes by size exclusion. With prolonged filtration, the size exclusion effect of the SNF/PDA⊂101 WTMs will become dominant. Therefore, the amount of small-molecule dyes that can be separated is far greater than the adsorption limit of the membranes. It is worth noting that the filter cake effect usually leads to a severe attenuation of the membrane water flux. However, our experiments confirmed that even after 24 h of filtering a Coomassie Brilliant Blue R solution with a concentration of 10 μM, the water flux of the 144-μm thick SNF/PDA⊂101(0) WTM was still 76.6 L h^{-1} m^{-2} bar^{-1}, which is still 10 times higher than current commercial ultrafiltration poly(vinylidene fluoride) membranes. Therefore, this result demonstrated that the formation of filter cake does not substantially affect the usability of SNF/PDA⊂101 WTMs.

Absorption of heavy metal ions, eutrophic elements, and radioactive elements by SNF/PDA⊂101 WTMs

Other types of SHPs that are present in low concentrations in sewage but cause considerable harm are heavy metal ions (e.g., mercury(II), lead(II), and chromium(IV) cations), eutrophic elements (e.g.,

Table 2. Separation and adsorption performance of SNF/PDA⊂101 WTMs for heavy metal ions

	IARC classification	Guideline for drinking water quality (mg L^{-1})	Removal capacity of SNF membrane	Removal capacity of SNF/PDA⊂101(0) WTM	Maximum removal capacity of SNF/PDA⊂101 WTMs	Potential recycle application
U^{3+}	Group 3	–	–	6.48 mg/g	15.72 mg/g	Energy
P	Group 1	–	–	8.12 mg/g	17.28 mg/g	Nutrient
Hg^{+}	Group 3	0.001	0.35 mg/g	6.04 mg/g	13.18 mg/g	Catalyst
Cd^{2+}	Group 1	0.01	3.2%	3.9%	5.1%	Electronics
As^{3+}	Group 1	0.05	0.005 mg/g	11.19 mg/g	35.00 mg/g	Semiconductor
Ni^{2+}	Group 1	0.07	1.8%	1.5%	2.5%	Magnetic
Cr^{6+}	Group 3	0.05	4.0%	4.8%	9.3%	Pigment
Pb^{2+}	Group 2A	0.07	0.56 mg/g	8.9 mg/g	13.63 mg/g	Catalyst

Table of the separation and adsorption performance of SNF/101 WTMs for heavy metal ions. IARC, International Agency for Research on Cancer.

phosphorus), and radioactive elements (e.g., uranium and phosphorus-32). Although the content of these SHPs is usually very low, they tend to accumulate in organisms and are highly toxic and carcinogenic.[70] Therefore, strictly limiting the concentration of these SHPs in drinking water is necessary. For instance, according to the WHO drinking water quality guidelines, the concentrations of mercury(II), nickel(II), chromium(III), and lead(II) cations should be lower than 0.002, 0.07, 0.05, and 0.07 mg L^{-1}, respectively (Table 2).[71]

It should be noted that PDA in SNF/PDA⊂101 WTMs is the dominant component for the absorption of these SHPs, so this study developed a series of SNF/PDA⊂101 WTMs by using MIL-101(Cr) or PDA⊂⋆ MIL-101(Cr) with different loading. By varying the PDA: MOF ratio, the polymer loading in MIL-101(Cr) can be systematically controlled to 18 and 22% (Figure S2D and Table S1). Continue to increase the amount of PDA during reaction, the embedded PDA loading is still maintained at 22%, which indicates that the PDA loading has reached the maximum in MOF pore. These complex membranes are named SNF/PDA⊂101(x) WTMs (x represents the PDA weight loading of PDA⊂MIL-101(Cr)).

As summarized in Table 2, SNF/PDA⊂101 WTMs can effectively remove phosphorus, mercury, arsenic, lead, and radioactive uranium ions. Specifically, the adsorption capacity of SNF/PDA⊂101(22) WTM for phosphorus, heavy metal ions, and uranium reached 17.3 mg g^{-1}, 35.0 mg g^{-1}, and 15.7 mg g^{-1}, respectively. The adsorption efficiency of SNF/PDA⊂101(22) WTM for heavy metal ions was three times higher than that of SNF/PDA⊂101(0) WTM. In addition, SNF/PDA⊂101(22) WTMs also removed chromium and cadmium with rejections of 9.3% and 5.1%, respectively (Figure 4A), which is comparable to the performance of oxidized multi-walled carbon nanotubes. By comparing the adsorption of these metal ions by different SNF/PDA⊂101 WTMs, it was confirmed that their adsorption capability for these metal ions depended on the load of PDA in PDA⊂MIL-101(Cr). Given the enhanced performance of the composite compared to the MOF, we established that the high density of the heavy metal-scavenging groups on the polymer backbone is the fundamental contributor to the high removal capacities. As summarized in Figure 4 and Table S5, the adsorption of heavy metal ions by SNF/PDA⊂101 WTMs increased gradually with the increase in PDA load. For example, SNF/PDA⊂101(22) WTM demonstrated the highest uranium removal capability with an absorption capacity of 15.7 mg g^{-1}, which was 2.4 times that of SNF/PDA⊂101(0) WTM. Similarly, the lead(II) cation adsorption capacity of SNF/PDA⊂101(22) WTM reached 13.6 mg g^{-1}, which was nearly twice that of SNF/PDA⊂101(0) WTM. The highest arsenic removal capacity was also found for SNF/PDA⊂101(22) WTM, and its adsorption efficiency (35.0 mg g^{-1}) was more than three times higher than that of SNF/PDA⊂101(0) WTM. The adsorption capacity of SNF/PDA⊂101(18) WTM for mercury(II) cations (13.18 mg g^{-1}) was more than twice of SNF/PDA⊂101(0) WTM. In comparison, SNF WTMs used under the same conditions could not adsorb these metal ions. It should be noted that the adsorption capacity was evaluated here by the vacuum filtration method. This procedure is too harsh for accurate adsorption measurements. Adsorption capacity evaluations normally use suspensions of adsorbents, exhibiting much larger specific surface areas and more adsorption sites than the solid membrane as the starting materials. The adsorption capacity will only be determined when the adsorption equilibrium is reached. By contrast, the effective contact area and interaction time of SHPs and membranes are very limited during vacuum filtration.

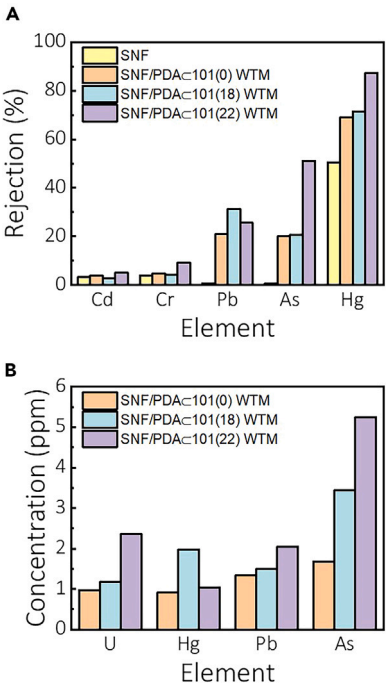

Figure 4. Separation performance of SNF/101 WTMs

(A) Rejection of 1-ppm heavy metal ion solutions over different SNF/101 WTMs.

(B) Adsorption concentration of 15-ppm SHP solutions over different SNF/101 WTMs.

General advantages of SNF/PDA⊂101 WTMs

The SNF/PDA⊂101 WTM boasts several advantages in separating various pollutants. First, its pore size range of 3–10 nm enables it to effectively remove nanoparticle pollutants through size exclusion. Second, the SNF protein component and MOF provide chemical sites for dye adsorption, making it highly effective in removing small-molecule dyes. Additionally, the embedded mesoporous PDA⊂MIL-101(Cr) nanoparticles adsorb heavy metal ions and radioactive elements due to the rich amino/imino and hydroxyl functional groups present in PDA. The heavy metal uptake exhibits a clear pH dependence, allowing SNF/PDA⊂101 WTMs to be regenerated by removing metal ions, and the reversibility can be detected using ascorbic acid and ethylenediaminetetraacetic acid.[29] Compared to other conventional WTMs, the integration of size-exclusion and adsorption capabilities enables the SNF/PDA⊂101 WTMs to be capable of removing a wide range of pollutants from sewage, including nanoparticles, small-molecule dyes, heavy metal ions, and radioactive elements, while also achieving a good removal capacity (Table S4).

Another critical advantage of SNF/PDA⊂101 WTMs is their low cost. The cost estimates and adsorbent capacities of the most studied nanomaterials are summarized in Figure 3I. SNF/PDA⊂101 WTMs exhibit an elegant tradeoff in terms of cost-saving and adsorbent capacity performance. For example, SNF/PDA⊂101(18) WTM cost about $0.86 per gram, comparable to cellulose nanomaterials ($0.65 to $2.80). However, SNF/PDA⊂101 WTMs exhibit superior adsorbent capacity compared to cellulose nanomaterials and a series of inorganic nanomaterials, such as graphene oxide, molybdenum disulfide, and tungsten disulfide. More importantly, SNF/PDA⊂101 WTMs also have considerable adsorption capacity for dyes and other SHPs and have the inherent size exclusion properties of ultrafiltration membranes. These advantages render the application value of SNF/PDA⊂101 WTMs much higher than that of adsorbent and ultrafiltration membranes, and these WTMs can be expected to become a practical and widespread new material for sewage treatment.

Conclusions

In summary, the present study reports on the fabrication and performance of low-cost WTMs with high water flux, obtained by the synergistic assembly of SNFs and PDA⊂MIL-101(Cr). These SNF/PDA⊂101 WTMs combine the size exclusion of nanoparticles with the strong adsorption of SHPs, thereby realizing the removal of a broad spectrum of pollutants from water. More specifically, the rejection of platinum nanoparticles of 3 nm in diameter by SNF/PDA⊂101 WTMs was as high as 100%. Furthermore, the rejection of

small-molecule dyes (0.8–2.4 nm in size) exceeded 94.5%. In addition, the mercury, arsenic, and lead adsorption capabilities of SNF/PDA⊂101 WTMs reached 13.2 mg g^{-1}, 35.0 mg g^{-1}, and 13.6 mg g^{-1}, respectively, and are comparable to the adsorption efficiencies of current commercial adsorbents. In addition, 100-μm thick SNF/PDA⊂101 WTMs can be formed from SNF/MOF dispersions in a short processing time (3 min) and can be manufactured into different types of WTMs, such as pressure-derived ultrafiltration membranes and syringe ultrafilters. Such diversity in the membrane formation methods, together with the high-water purification efficiency of the resultant membranes, essentially expands the applications of SNF/PDA⊂101 WTMs in water treatment, the food industry, and life sciences.

Limitations of the study

The PDA in SNF/PDA⊂101 WTMs is the dominant component for the absorption of these SHPs. It is reasonable to speculate that with the increase of PDA loading, the rejection rate of heavy metal ions will be improved, which have not been fully investigated in this work apart from solid PDA⊂101 reported herein. According to the ideas of this article, building hollow structures to improve water purification efficiency could be further studied.

STAR★METHODS

Detailed methods are provided in the online version of this paper and include the following:

- KEY RESOURCES TABLE
- RESOURCE AVAILABILITY
  - Lead contact
  - Materials availability
  - Data and code availability
- METHOD DETAILS
  - Section S1. Synthesis
  - Section S2. Equation
  - Section S3. Characterization

SUPPLEMENTAL INFORMATION

Supplemental information can be found online at https://doi.org/10.1016/j.isci.2023.107290.

ACKNOWLEDGMENTS

This work was sponsored by the National Natural Science Foundation of China (Nos. 21935002, 51973116, 52003156, 22075181), the starting grant of ShanghaiTech University and the double first-class initiative fund of ShanghaiTech University. The authors thank the staff members from Analytical Instrumentation Center (#SPST-AIC10112914), and the Center for High resolution Electron Microscopy (CħEM), SPST, ShanghaiTech University for assistance during data collection. The authors also thank Professor Lien-Yang Chou, Piao Wen, Hao Zhang and Chenxi Zhao for the kind help during the experiment.

AUTHOR CONTRIBUTIONS

S.L. and T.L. conceived and developed this study. X.Z. and C.W. performed the experiments and analyzed the data. D.D. carried out N_2 adsorption measurements and EDS, and draw the scheme images. The manuscript was written by X.Z. and S.L. with input from all authors. J.R. polished and submitted manuscript.

DECLARATION OF INTERESTS

The authors declare no competing interests.

Received: March 16, 2023
Revised: May 9, 2023
Accepted: July 3, 2023
Published: July 11, 2023

REFERENCES

1. Tchounwou, P.B., Yedjou, C.G., Patlolla, A.K., and Sutton, D.J. (2012). Heavy metal toxicity and the environment. Exp. Suppl. *101*, 133–164.
2. Shadabi, L., and Ward, F.A. (2022). Predictors of Access to Safe Drinking Water: Policy Implications (Water Policy).
3. Ritchie, H., and Roser, M. (2021). Clean Water and Sanitation. Our World in Data.
4. Gleick, P.H. (2003). Global freshwater resources: soft-path solutions for the 21st century. Science *302*, 1524–1528.
5. United Nations World Water Development (2015). Water for a Sustainable World, the United Nations World Water Development Report (Paris: United Nations Educational, Scientific and Cultural Organization).
6. Shannon, M.A., Bohn, P.W., Elimelech, M., Georgiadis, J.G., Marinas, B.J., and Mayes, A.M. (2010). Science and technology for water purification in the coming decades. Nature *452*, 301–310.
7. Vandezande, P., Gevers, L.E.M., and Vankelecom, I.F.J. (2008). Solvent resistant nanofiltration: separating on a molecular level. Chem. Soc. Rev. *37*, 365–405.
8. Werber, J.R., Osuji, C.O., and Elimelech, M. (2016). Materials for next-generation desalination and water purification membranes. Nat. Rev. Mater. *1*, 16018.
9. Krieg, E., Weissman, H., Shirman, E., Shimoni, E., and Rybtchinski, B. (2011). A recyclable supramolecular membrane for size-selective separation of nanoparticles. Nat. Nanotechnol. *6*, 141–146.
10. GenáZhang, Q., LuáHan, G., MeiáZhu, A., LináLiu, Q., Zhu, A.M., and Liu, Q.L. (2013). Ultrathin self-assembled anionic polymer membranes for superfast size-selective separation. Nanoscale *5*, 11028–11034.
11. Liang, B., Wang, H., Shi, X., Shen, B., He, X., Ghazi, Z.A., Khan, N.A., Sin, H., Khattak, A.M., Li, L., and Tang, Z. (2018). Microporous membranes comprising conjugated polymers with rigid backbones enable ultrafast organic-solvent nanofiltration. Nat. Chem. *10*, 961–967.
12. Bolisetty, S., and Mezzenga, R. (2016). Amyloid–carbon hybrid membranes for universal water purification. Nat. Nanotechnol. *11*, 365–371.
13. Ling, S., Jin, K., Kaplan, D.L., and Buehler, M.J. (2016). Ultrathin free-standing Bombyx mori silk nanofibril membranes. Nano Lett. *16*, 3795–3800.
14. Peng, X., Jin, J., Nakamura, Y., Ohno, T., and Ichinose, I. (2009). Ultrafast permeation of water through protein-based membranes. Nat. Nanotechnol. *4*, 353–357.
15. Qiu, B., Tao, X., Wang, H., Li, W., Ding, X., and Chu, H. (2021). Biochar as a low-cost adsorbent for aqueous heavy metal removal: a review. J. Anal. Appl. Pyrol. *155*, 105081.
16. Striemer, C.C., Gaborski, T.R., McGrath, J.L., and Fauchet, P.M. (2007). Charge-and size-based separation of macromolecules using ultrathin silicon membranes. Nature *445*, 749–753.
17. Choi, H., Sofranko, A., and Dionysiou, D. (2006). Nanocrystalline TiO2 photocatalytic membranes with a hierarchical mesoporous multilayer structure: synthesis, characterization, and multifunction. Adv. Funct. Mater. *16*, 1067–1074.
18. Sun, L., Ying, Y., Huang, H., Song, Z., Mao, Y., Xu, Z., and Peng, X. (2014). Ultrafast molecule separation through layered WS2 nanosheet membranes. ACS Nano *8*, 6304–6311.
19. Sun, L., Huang, H., and Peng, X. (2013). Laminar MoS 2 membranes for molecule separation. Chem. Commun. *49*, 10718–10720.
20. Joshi, R.K., Carbone, P., Wang, F.-C., Kravets, V.G., Su, Y., Grigorieva, I.V., Wu, H.A., Geim, A.K., and Nair, R.R. (2014). Precise and ultrafast molecular sieving through graphene oxide membranes. Science *343*, 752–754.
21. Lee, Y.M., Jung, B., Kim, Y.H., Park, A.R., Han, S., Choe, W.S., and Yoo, P.J. (2014). Nanomesh-structured ultrathin membranes harnessing the unidirectional alignment of viruses on a graphene-oxide film. Adv. Mater. *26*, 3899–3904.
22. Huang, H., Song, Z., Wei, N., Shi, L., Mao, Y., Ying, Y., Sun, L., Xu, Z., and Peng, X. (2013). Ultrafast viscous water flow through nanostrand-channelled graphene oxide membranes. Nat. Commun. *4*, 2979.
23. Gao, S.J., Qin, H., Liu, P., and Jin, J. (2015). SWCNT-intercalated GO ultrathin films for ultrafast separation of molecules. J. Mater. Chem. A Mater. *3*, 6649–6654.
24. Liang, H.W., Wang, L., Chen, P.Y., Lin, H.T., Chen, L.F., He, D., and Yu, S.H. (2010). Carbonaceous nanofiber membranes for selective filtration and separation of nanoparticles. Adv. Mater. *22*, 4691–4695.
25. Wang, C., Liu, X., Chen, J.P., and Li, K. (2015). Superior removal of arsenic from water with zirconium metal-organic framework UiO-66. Sci. Rep. *5*, 16613.
26. Guo, Y., Jia, Z., Shi, Q., Liu, Z., Wang, X., and Li, L. (2019). Zr (IV)-based coordination porous materials for adsorption of Copper (II) from water. Microporous Mesoporous Mater. *285*, 215–222.
27. Abdelmoaty, A.S., El-Wakeel, S.T., Fathy, N., and Hanna, A.A. (2022). High performance of UiO-66 metal–organic framework modified with melamine for uptaking of lead and cadmium from aqueous solutions. J. Inorg. Organomet. Polym. Mater. *32*, 2557–2567.
28. Jian, M., Liu, B., Zhang, G., Liu, R., and Zhang, X. (2015). Adsorptive removal of arsenic from aqueous solution by zeolitic imidazolate framework-8 (ZIF-8) nanoparticles. Colloids Surf. A Physicochem. Eng. Asp. *465*, 67–76.
29. Sun, D.T., Peng, L., Reeder, W.S., Moosavi, S.M., Tiana, D., Britt, D.K., Oveisi, E., and Queen, W.L. (2018). Rapid, selective heavy metal removal from water by a metal–organic framework/polydopamine composite. ACS Cent. Sci. *4*, 349–356.
30. Sun, D.T., Gasilova, N., Yang, S., Oveisi, E., and Queen, W.L. (2018). Rapid, selective extraction of trace amounts of gold from complex water mixtures with a metal–organic framework (MOF)/polymer composite. J. Am. Chem. Soc. *140*, 16697–16703.
31. Liu, R., Chi, L., Wang, X., Wang, Y., Sui, Y., Xie, T., and Arandiyan, H. (2019). Effective and selective adsorption of phosphate from aqueous solution via trivalent-metals-based amino-MIL-101 MOFs. Chem. Eng. J. *357*, 159–168.
32. Guillem-Navajas, A., Martín-Illán, J.Á., Salagre, E., Michel, E.G., Rodriguez-San-Miguel, D., and Zamora, F. (2022). Iron oxyhydroxide-covalent organic framework nanocomposite for efficient as (III) removal in water. ACS Appl. Mater. Interfaces *14*, 50163–50170.
33. Wang, M., Zhang, P., Liang, X., Zhao, J., Liu, Y., Cao, Y., Wang, H., Chen, Y., Zhang, Z., Pan, F., et al. (2022). Ultrafast seawater desalination with covalent organic framework membranes. Nat. Sustain. *5*, 518–526.
34. Khan, N.A., Zhang, R., Wang, X., Cao, L., Azad, C.S., Fan, C., Yuan, J., Long, M., Wu, H., Olson, M.A., and Jiang, Z. (2022). Assembling covalent organic framework membranes via phase switching for ultrafast molecular transport. Nat. Commun. *13*, 3169.
35. Wu, C., Zhang, K., Wang, H., Fan, Y., Zhang, S., He, S., Wang, F., Tao, Y., Zhao, X., Zhang, Y.-B., et al. (2020). Enhancing the gas separation selectivity of mixed-matrix membranes using a dual-interfacial engineering approach. J. Am. Chem. Soc. *142*, 18503–18512.
36. Wang, D., Li, S., Wu, C., and Li, T. (2022). Surface-seal encapsulation of a homogeneous catalyst in a mesoporous metal–organic framework. J. Am. Chem. Soc. *144*, 685–689.
37. Eguizábal, A., Sgroi, M., Pullini, D., Ferain, E., and Pina, M. (2014). Nanoporous PBI membranes by track etching for high temperature PEMs. J. Membr. Sci. *454*, 243–252.
38. Mourhatch, R., Tsotsis, T.T., and Sahimi, M. (2010). Network model for the evolution of the pore structure of silicon-carbide membranes during their fabrication. J. Membr. Sci. *356*, 138–146.
39. Karan, S., Samitsu, S., Peng, X., Kurashima, K., and Ichinose, I. (2012). Ultrafast viscous permeation of organic solvents through diamond-like carbon nanosheets. Science *335*, 444–447.
40. Joseph, N., Ahmadiannamini, P., Hoogenboom, R., and Vankelecom, I.F.J. (2014). Layer-by-layer preparation of

polyelectrolyte multilayer membranes for separation. Polym. Chem. *5*, 1817–1831.

41. Zhang, B., Li, X., Zou, J., and Kim, F. (2020). MnCO3 on graphene porous framework via diffusion-driven layer-by-layer assembly for high-performance pseudocapacitor. ACS Appl. Mater. Interfaces *12*, 47695–47703.

42. Dai, D., Wang, H., Li, C., Qin, X., and Li, T. (2021). A physical entangling strategy for simultaneous interior and exterior modification of metal–organic framework with polymers. Angew. Chem. *60*, 7389–7396.

43. Li, H., Zhou, X.Y., Yang, X.R., Zhu, Y.G., Hong, Y.W., Su, J.Q., and Xue, Q. (2019). High-efficiency separation performance of oil-water emulsions of polyacrylonitrile nanofibrous membrane decorated with metal-organic frameworks. Sci. Total Environ. *665*, 61–68.

44. Fan, Y., Liang, H., Jian, M., Liu, R., Zhang, X., Hu, C., and Liu, H. (2023). Removal of dimethylarsinate from water by robust NU-1000 aerogels: Impact of the aerogel materials. Chem. Eng. J. *455*, 140387.

45. Ji, C., Ren, Y., Yu, H., Hua, M., Lv, L., and Zhang, W. (2022). Highly efficient and selective Hg (II) removal from water by thiol-functionalized MOF-808: kinetic and mechanism study. Chem. Eng. J. *430*, 132960.

46. Wu, C., Dai, D., Zhao, X., Wang, H., and Li, T. (2022). One-step rapid fabrication of MOF@ polymer core–shell particles through non-solvent induced surface deposition. J. Mater. Chem. A Mater. *10*, 24676–24684.

47. Ling, S., Qin, Z., Huang, W., Cao, S., Kaplan, D.L., and Buehler, M.J. (2017). Design and function of biomimetic multilayer water purification membranes. Sci. Adv. *3*, e1601939.

48. Peng, L., Yang, S., Sun, D.T., Asgari, M., and Queen, W.L. (2018). MOF/polymer composite synthesized using a double solvent method offers enhanced water and CO 2 adsorption properties. Chem. Commun. *54*, 10602–10605.

49. Zorainy, M.Y., Gar Alalm, M., Kaliaguine, S., and Boffito, D.C. (2021). Revisiting the MIL-101 metal–organic framework: design, synthesis, modifications, advances, and recent applications. J. Mater. Chem. A Mater. *9*, 22159–22217.

50. Henschel, A., Gedrich, K., Kraehnert, R., and Kaskel, S. (2008). Catalytic properties of MIL-101. Chem. Commun. 4192–4194.

51. Férey, G., Mellot-Draznieks, C., Serre, C., Millange, F., Dutour, J., Surblé, S., and Margiolaki, I. (2005). A chromium terephthalate-based solid with unusually large pore volumes and surface area. Science *309*, 2040–2042.

52. Knight, A.S., Zhou, E.Y., Pelton, J.G., and Francis, M.B. (2013). Selective chromium (VI) ligands identified using combinatorial peptoid libraries. J. Am. Chem. Soc. *135*, 17488–17493.

53. Jalayeri, H., Aprea, P., Caputo, D., Peluso, A., and Pepe, F. (2020). Synthesis of amino-functionalized MIL-101 (Cr) MOF for hexavalent chromium adsorption from aqueous solutions. Environ. Nanotechnol. Monit. Manag. *14*, 100300.

54. Vo, T.K., Trinh, T.P., Nguyen, V.C., and Kim, J. (2021). Facile synthesis of graphite oxide/MIL-101 (Cr) hybrid composites for enhanced adsorption performance towards industrial toxic dyes. J. Ind. Eng. Chem. *95*, 224–234.

55. Liu, L., Fang, Y., Meng, Y., Wang, X., Ma, F., Zhang, C., and Dong, H. (2020). Efficient adsorbent for recovering uranium from seawater prepared by grafting amidoxime groups on chloromethylated MIL-101 (Cr) via diaminomaleonitrile intermediate. Desalination *478*, 114300.

56. Liu, Y., Ai, K., and Lu, L. (2014). Polydopamine and its derivative materials: synthesis and promising applications in energy, environmental, and biomedical fields. Chem. Rev. *114*, 5057–5115.

57. He, S., Chen, L., Cui, J., Yuan, B., Wang, H., Wang, F., Yu, Y., Lee, Y., and Li, T. (2019). General way to construct micro-and mesoporous metal–organic framework-based porous liquids. J. Am. Chem. Soc. *141*, 19708–19714.

58. Zangmeister, R.A., Morris, T.A., and Tarlov, M.J. (2013). Characterization of polydopamine thin films deposited at short times by autoxidation of dopamine. Langmuir *29*, 8619–8628.

59. Rockwood, D.N., Preda, R.C., Yücel, T., Wang, X., Lovett, M.L., and Kaplan, D.L. (2011). Materials fabrication from Bombyx mori silk fibroin. Nat. Protoc. *6*, 1612–1631.

60. Baker, R.W. (2012). Membrane Technology and Applications (John Wiley & Sons).

61. Lin, N., and Liu, X.Y. (2015). Correlation between hierarchical structure of crystal networks and macroscopic performance of mesoscopic soft materials and engineering principles. Chem. Soc. Rev. *44*, 7881–7915.

62. Zhang, Q., Ghosh, S., Samitsu, S., Peng, X., and Ichinose, I. (2011). Ultrathin freestanding nanoporous membranes prepared from polystyrene nanoparticles. J. Mater. Chem. *21*, 1684–1688.

63. Zhang, Q.G., Deng, C., Soyekwo, F., Liu, Q.L., and Zhu, A.M. (2016). Sub-10 nm wide cellulose nanofibers for ultrathin nanoporous membranes with high organic permeation. Adv. Funct. Mater. *26*, 792–800.

64. Schäfer, A., Fane, A.G., and Waite, T.D. (2005). Nanofiltration: Principles and Applications (Elsevier).

65. Lu, Y., Suzuki, T., Zhang, W., Moore, J.S., and Mariñas, B.J. (2007). Nanofiltration membranes based on rigid star amphiphiles. Chem. Mater. *19*, 3194–3204.

66. Braeken, L., Van der Bruggen, B., and Vandecasteele, C. (2006). Flux decline in nanofiltration due to adsorption of dissolved organic compounds: model prediction of time dependency. J. Phys. Chem. B *110*, 2957–2962.

67. Namasivayam, C., and Kadirvelu, K. (1999). Uptake of mercury (II) from wastewater by activated carbon from an unwanted agricultural solid by-product: coirpith. Carbon *37*, 79–84.

68. Naseem, R., and Tahir, S.S. (2001). Removal of Pb (II) from aqueous/acidic solutions by using bentonite as an adsorbent. Water Res. *35*, 3982–3986.

69. Huang, T., Moosa, B.A., Hoang, P., Liu, J., Chisca, S., Zhang, G., AlYami, M., Khashab, N.M., and Nunes, S.P. (2020). Molecularly-porous ultrathin membranes for highly selective organic solvent nanofiltration. Nat. Commun. *11*, 5882.

70. International Agency for Research on Cancer (2012). Agents Classified by the IARC Monographs, pp. 1–104. http://monographs.iarc. fr/ENG/Classification/index. php.

71. WHO (2011). Guidelines for Drinking-Water Quality, *216* (World Health Organization), pp. 303–304.

72. Tsung, C.-K., Kuhn, J.N., Huang, W., Aliaga, C., Hung, L.-I., Somorjai, G.A., and Yang, P. (2009). Sub-10 nm platinum nanocrystals with size and shape control: catalytic study for ethylene and pyrrole hydrogenation. J. Am. Chem. Soc. *131*, 5816–5822.

73. Lu, G., Li, S., Guo, Z., Farha, O.K., Hauser, B.G., Qi, X., Wang, Y., Wang, X., Han, S., Liu, X., et al. (2012). Imparting functionality to a metal–organic framework material by controlled nanoparticle encapsulation. Nat. Chem. *4*, 310–316.

74. Ostadfar, A. (2016). Biofluid Mechanics: Principles and Applications (Academic Press).

75. Li, B., Zhang, Y., Ma, D., Shi, Z., and Ma, S. (2014). Mercury nano-trap for effective and efficient removal of mercury (II) from aqueous solution. Nat. Commun. *5*, 5537.

STAR★METHODS

KEY RESOURCES TABLE

REAGENT or RESOURCE	SOURCE	IDENTIFIER
Chemicals, peptides, and recombinant proteins		
Chromium (III) nitrate nonahydrate	Aladdin	CAS: 7789-02-8
1,4-dicarboxybenzene	Aladdin	CAS: 100-21-0
lithium bromide	Greagent	CAS: 7447-41-8
Eosin B	Aladdin	CAS: 56360-46-4
Alcian blue 8GX	Aladdin	CAS: 33864-99-2
Congo red	Aladdin	CAS: 573-58-0
Rhodamine B	Aladdin	CAS: 81-88-9
Chloroplatinic acid hexahydrate	Macklin	CAS: 18497-13-7
Ammonium tetrachloroplatinate	Macklin	CAS: 13820-41-2
tetramethylammonium bromide	Alfa Aesar	CAS: 64-20-0
polyvinylpyrrolidone	Alfa Aesar	CAS: 9003-39-8
gold chloride solution	Aladdin	CAS: 16903-35-8
trisodium citrate	Fisher Scientific	CAS: 6132-04-3
N, N-dimethylformamide	Greagent	CAS: 68-12-2
MIL-101	CCDS	605510

RESOURCE AVAILABILITY

Lead contact

Further information and requests for resources and reagents should be directed to and will be fulfilled by the lead contact, Prof. Shengjie Ling (lingshj@shanghaitech.edu.cn).

Materials availability

Raw materials used in the study are commercially available.

Data and code availability

- The crystal data of The MIL-101 have been deposited at the Cambridge Crystallographic Data Center (CCDC) and are publicly available as of the date of publication. Accession numbers are listed in the key resources table.
- This paper does not report original code.
- Any additional information required to reanalyze the data reported in this paper is available from the lead contact upon request.

METHOD DETAILS

Section S1. Synthesis

Synthesis of MIL-101(Cr)

MIL-101(Cr) was synthesized by dissolving 1.57 g $Cr(NO_3)_3 \cdot 9H_2O$ and 0.66 g H_2BDC in 60 mL H_2O, and heated at 180°C for 8 h.

Synthesis of PDA⊂MIL-101(Cr)

PDA⊂MIL-101(Cr) was synthesized according to the reported double solvent method.[48] MIL-101(Cr) powder (130 mg) was heated at 130°C under a vacuum overnight. Then, 10 mL *n*-hexane was added to the powder under sonication. After stirring for 30 min, 0.228 mL of an aqueous dopamine hydrochloride solution

with varying concentrations (for PDA⊂101(18): 0.513 M, PDA⊂101(21): 1.026 M, PDA⊂101(22): 2.052 M) was added and stirring continued for 1 h. Then, the supernatant was removed and the remaining suspension was centrifuged to isolate the modified powder. To the solid, 20 mL ethanol, 45 mL water, and 375 μL aqueous ammonia solution was added followed by stirring for 9 h.

Degumming of B. mori silk

The Bombyx mori (B. mori) cocoon silk fiber were boiled twice in an aqueous solution of 0.5% (w/w) $NaHCO_3$ for 30 min. Subsequently, the degummed silk fibers were washed with 4 L deionized water and then dried in an oven at 60°C overnight.

Preparation of SNF solution

In a typical process, 5 g degummed silk fiber was stirred in 0.05 mL of a 9.3 M aqueous LiBr solution at 64.5°C for 3 h until there was no agglomeration and precipitation. The solution was cooled to room temperature and dialyzed against deionized water. Then a 2% (wt%) silk fibroin solution is obtained after dialysis for 72 h.

Preparation of SNF/PDA⊂101 WTMs by filtration and self-assembly

An aqueous solution containing 0.5 mg mL^{-1} SNF and MOF particles were passed through a polycarbonate filter membrane (pore size of 0.22 μm, diameter of 25 mm, Millipore), achieving the self-assembly of composite membranes to obtain SNF/PDA⊂101 WTMs on polycarbonate filtration membranes.

Synthesis of 3 nm Pt nanoparticles (NPs)

Pt NPs were synthesized according to the reported method.[72] Firstly, dissolving PVP (277.85 mg) and $H_2PtCl_6 \cdot 6H_2O$ (64.75 mg) in 21.25 mL EG. Then, the mixture was heated to 200°C in an oil bath under a nitrogen atmosphere with magnetic stirring (350 rpm). When the color of the solution changes to black, 3.75 mL 0.5 M TMABr EG solution was added to the mixture to continue stirring for 20 min. After cooling to room temperature, acetone (90 mL) was added to form a cloudy black suspension, which was separated by centrifugation. The black product was collected by discarding the colorless supernatant. The products were further washed three times by precipitation/dissolution (redispersed in 20 mL of ethanol and then precipitated by adding 80 mL of hexanes). The nanocrystals were then redispersed in 25 mL of DMF for later use.

Synthesis of 10 nm Pt nanoparticles (NPs)

Pt NPs were synthesized according to the reported method.[72] Firstly, dissolving PVP (277.85 mg), $(NH_4)_2Pt(II)Cl_4$ (46.63 mg) in 21.25 mL EG. Then, the mixture was heated to 200°C in an oil bath under a nitrogen atmosphere with magnetic stirring (350 rpm). When the color of the solution changed to black, 3.75 mL 0.5 M TMABr EG solution was added to the mixture to continue stirring for 20 min. After cooling down to room temperature, acetone (90 mL) was added to form a cloudy black suspension, which was separated by centrifugation. The black product was collected by discarding the colorless supernatant. The products were further washed three times by precipitation/dissolution (redispersed in 20 mL of ethanol and then precipitated by adding 80 mL of hexanes). The nanocrystals were then redispersed in 25 mL of DMF for later use.

Synthesis of PVP-stabilized 15.5 nm Au nanoparticles (NPs)

15.5 nm Au nanoparticles (NPs) were prepared by a sodium citrate reduction method of $HAuCl_4$.[73] An aqueous solution of $HAuCl_4$ (0.01%, 150 ml) was brought to a vigorous boil with rapid stirring in a 250 mL round bottom flask fitted with a reflux condenser. When the solution started to boil, an aqueous solution of trisodium citrate (1%, 4.5 ml) was added. The mixture was refluxed by stirring for another 20 minutes. The resulting deep red suspension was then removed from the heat. After the Au NP sol was cooled to room temperature, a solution of PVP (0.5 g) in water (20 ml) was added dropwise to the Au NP sol with stirring, and the mixture was further stirred at room temperature for 24 hours. The Au NPs were collected by centrifugation at 14,000 rpm for 30 minutes and washed with anhydrous methanol three times.

Section S2. Equation

(1) Hagen-Poiseuille equation

The classical Hagen–Poiseuille equation[74] is fit for a homogeneous membrane with uniform channels:

$$f_{flux} = \frac{Q}{A\Delta P} = \frac{\pi\beta r^4}{8\mu H} \quad \text{(Equation 1)}$$

Thus, it was clear that $f_{flux} \sim H^{-1}$ and it was shown that having the two composites in the SNF-MOF composite helped to maintain the flux once the membrane was thicker than the membrane made of pure SNF. It was noted that β relates to the membrane porosity and pore shape and its numerical value was determined by fitting according to the *flux-H* relationship. Therefore, for pure SNF membrane its β and *r* values would be probably very different from those of the SNF/MOF assembly. It was the interaction between SNF and MOF that made the combination more water permeable, as the pure SNF membrane had much weaker water permeability than the SNF/MOF membrane of the same thickness.

(2) Separation performance measurement

The separation performance is performed on the vacuum filter device (glass vacuum filter assembly device, membrane diameter is 25 mm, funnel top inner diameter is 15 mm). The water (10 mL) is filtered onto the membrane to measure the pure water flux (L h^{-1} m^{-2} bar^{-1}). The calculation formula is J = V/(Atp), where V is the volume of filtered water (L), A is the effective membrane filtration area (m^2), t is the filtration time (h) and p is the pressure through the membrane (bar). Dyes, nanoparticles, and heavy metal ion solutions were used to evaluate the filtration effect of the membrane. The feed (5 mL) was filtered at 80 KPa. The calculation formula for the filtration effect[47,75] is as follows:

$$R = \left(1 - \frac{C_p}{C_f}\right) \times 100\% \quad \text{(Equation 2)}$$

C_f and C_p are the concentrations of compounds in the feed and filtrate, respectively.

Interception rate (R, %) calculated by the optical density value measured by enzyme marker and concentration of elements tested by ICP-OES.

Section S3. Characterization

The powder X-ray diffraction (PXRD) spectra were obtained using an X-ray diffractometer (Bruker D8) ranging from 3° to 30° with Cu-Kα radiation (40 mA; 40 kV). Transmission electron microscope (TEM) images and energy dispersive X-ray spectroscopy (EDS) mapping images of the MOFs were acquired on a JEM 1400 field-emission transmission electron microscope with the voltage set at 120 kV. Scanning electron microscope (SEM) images were acquired on a JEOL JSM 7800F Prime SEM. Inductively coupled plasma-optical emission spectroscopy (ICP-OES) experiments were carried out on a Thermo-Fisher ICP-OES Icap 7400. TGA experiments were performed on a PerkinElmer TGA 8000. FT-IR spectra were performed on a PerkinElmer FTIR spectrometer in transmission mode in the range of 4000-400 cm^{-1}. The morphological structures of the SNFs were recorded using Bruker dimension ICON AFM. X-ray photoelectron spectroscopy (XPS) data were determined by Thermo Fisher ESCALAB 250 Xi. N_2 adsorption-desorption isotherms were performed on BELSORP-max.

Adsorption experiments

The adsorption experiments were carried out to evaluate the adsorption performance of dyes and heavy metals on the SNF/PDA⊂101 composites. Dye aqueous solution is prepared by deionized water, heavy metal ions, and radioactive isotope aqueous solution is prepared by deionized water dilution standard solution. Diluting high-concentration aqueous solution to obtain different concentrations of the solution, used in various experiments. In these experiments, the freshly prepared SNF/PDA⊂101 WTMs were filtrated SHP aqueous solutions under a very low rate (1.2 mL/h) using a syringe pump to reach adsorption equilibrium.